Colloidal electrolyte friction: the effect of finite-sized electrolyte ions

2004 J. Phys.: Condens. Matter 16 S4021

(http://iopscience.iop.org/0953-8984/16/38/018)

INSTITUTE OF PHYSICS PUBLISHING JOURNAL OF PHYSICS: CONDENSED MATTER

J. Phys.: Condens. Matter **16** (2004) S4021–S4038 PII: S0953-8984(04)78939-0

Colloidal electrolyte friction: the effect of finite-sized electrolyte ions

Mathieu G McPhie and Gerhard Nägele

Institut für Festkörperforschung, Teilinstitut Weiche Materie, Forschungszentrum Jülich, D-52425 Jülich, Germany

E-mail: g.naegele@fz-juelich.de

Received 5 April 2004
Published 10 September 2004
Online at stacks.iop.org/JPhysCM/16/S4021
doi:10.1088/0953-8984/16/38/018

Abstract

The electro-hydrodynamic coupling of electrolyte ions and surface-dissociated counterions, i.e., microions, to the motion of a suspended colloidal macroion leads to an additional contribution to the colloidal friction coefficient. On the basis of the primitive model and the generalized Smoluchowski diffusion equation, a simplified mode–mode coupling scheme (MCS) is developed for quantifying the effect of electrolyte friction on the tracer diffusion of a macroion. In this scheme, far-field hydrodynamic interactions between all ionic species are considered. The influence of the finite size of the microions is accounted for by using mean spherical approximation expressions of static pair correlation functions for unequal sizes. The present paper extends earlier work of one of the authors to include the effects of finite-sized and hydrodynamically interacting microions. Our theoretical results are used to test the relevance of finite size effects in suspensions of nano-sized particles such as charged globular micelles. Significant finite size effects are only observed for macroion–microion size ratios typically smaller than 10.

1. Introduction

The dynamics of charge-stabilized colloidal particles of globular shape (so-called macroions) dispersed in a solution of weakly charged counter- and co-ions forming a neutralizing and screening microion atmosphere, has attracted considerable interest, both from the experimental and theoretical point of view. The reason for the strong interest in these systems is that a large fraction of colloidal systems of biological and technological relevance are, in fact, charge-stabilized dispersions with water as solvent. A theoretical description of the transport properties in these systems is demanding, since the particle dynamics is determined by a delicate interplay of electrostatic, steric and solvent-mediated hydrodynamic forces. Existing theoretical work on the dynamics of charge-stabilized colloids is mostly based on an effective

macrofluid model of dressed macroions which interact by an effective pair potential of spherical symmetry. The effective pair potential has been determined on various levels of approximation, ranging from mean-field schemes to more sophisticated integral equation approaches, density functional theory approximations and computer simulations, by integrating out the microionic degrees of freedom. To date, the electrostatic part of the celebrated Derjaguin–Landau–Vervey–Overbeek (DLVO) potential of linear electrostatic screening is still the most widely used effective macroion pair potential. Here, the presence of the screening microions is manifest in a mean-field-like way through a screening parameter κ and an effective macroion charge [1, 2].

A major drawback of the dressed macroion model with spherically symmetric pair potential is that it does not account for the kinetic influence of the microionic atmosphere on the dynamics of the colloidal particles. The thermal fluctuations in the microionic density surrounding a colloidal macroion are coupled to its Brownian motion by electro-steric ion–ion interactions and by solvent-mediated hydrodynamic interactions (HI). An explicit inclusion of HI effects between all ionic species demands the use of a more fundamental level of description where the macroions and the microions are treated on an equal footing as separate dynamical entities. The simplest model with such a democratic treatment of microions and macroions is given by a dynamic extension of the primitive model (PM) [3]. In this extended model, all ions are described as uniformly charged hard spheres interacting by long-range Coulomb forces, embedded in an unstructured solvent of uniform dielectric constant ϵ and shear viscosity η_0. The local solvent flow, in response to the motion of the ionic spheres, is described by the Stokes equation of low Reynold's number creeping flow.

An interesting example of an electrokinetic effect caused by the dynamic coupling of the microions to the macroion motion is the tracer diffusion of a spherical colloidal macroion in an unbounded multi-component electrolyte. Light scattering data have revealed, in this case, that the diffusive motion of the electrolyte ions relative to the large tracer macroion leads to an increase in the friction coefficient of the tracer [4, 5]. A consequence of the electrolyte friction is that the long-time self-diffusion coefficient of the tracer,

$$D_{\mathrm{T}}^{\mathrm{L}} = \frac{k_{\mathrm{B}}T}{\zeta_{\mathrm{T}}^{\mathrm{S}} + \Delta\zeta_{\mathrm{T}}}, \tag{1}$$

has a minimal value when the thickness of the macroionic cloud, as measured by the Debye screening length κ^{-1}, is approximately equal to the diameter, $\sigma_{\mathrm{T}} = 2a_{\mathrm{T}}$, of the tracer sphere. Here, $\zeta_{\mathrm{T}}^{\mathrm{S}} = k_{\mathrm{B}}T/D_{\mathrm{T}}^{\mathrm{S}}$ is the friction coefficient related to the short-time tracer-diffusion coefficient $D_{\mathrm{T}}^{\mathrm{S}}$. It is, in general, different from the bare friction coefficient, ζ_{T}^{0}, of an isolated sphere, due to the hydrodynamic interactions between the tracer sphere and the microions. The long-time increase in the tracer friction caused by the electrolyte is quantified by the excess friction contribution $\Delta\zeta_{\mathrm{T}}$.

In recent work, Nägele and Dhont [6] and Kollmann and Nägele [7, 8] have formulated a multi-component mode–mode coupling scheme (MCS) for the overdamped Brownian motion of spherical particles based on the many-body Smoluchowski equation. In this scheme, HI between macroions and microions are treated on a pairwise additive level using the long-distance Rotne–Prager (RP) form of the hydrodynamic mobility tensors, with all ionic species described by the dynamically extended primitive model. In [7, 8], the microions had been considered as point-like with regard to their excluded volume interactions, characterized, however, by finite values of the free diffusion coefficients. For analytic simplicity, the static pair correlation functions required as input to the MCS had been determined by the linear Debye–Hückel (DH) approximation. Explicit analytic expressions have been derived in this way for the (time-resolved) electrolyte friction contribution to $D_{\mathrm{T}}^{\mathrm{L}}$ and to the sedimentation velocity

of the tracer in a many-component electrolyte solution. These results have been shown to be in good accord with experimental results for D_T^L in dilute suspensions of polystyrene spheres and with Booth's theory of macroion sedimentation [9, 10]. An important conclusion obtained in [7] is that the minimum in D_T^L at $\kappa a_T \approx 0.3$ is due to the combined effect of hydrodynamic and electro-steric forces acting between macroions and microions. The minimum cannot be explained by the presence of direct forces alone, as it has been attempted in earlier statistical mechanical approaches where HI are totally ignored [11–16].

In this paper, we generalize earlier results on electrolyte friction by Kollmann and Nägele to finite-sized macroions. We will show that microionic finite size effects are only relevant for suspensions of nano-sized macroions such as charged globular proteins or micelles [17, 18], when the size ratio, $\lambda = a_T/a_s$, between the macroion and small microion radii is typically less than 10. The inclusion of finite microionic sizes allows us to explore an extended range of diffusion problems, from the tracer diffusion of a large colloidal macroion down to self-diffusion in genuine salt solutions. In addition to the macroion–microion HI, we further account for HI among the microions. In [7], microion–microion HI had been neglected in comparison to the strong HI acting between the large macroion and the surrounding microions. As input for the static pair correlation functions, we use analytic expressions provided by the mean spherical approximation (MSA) solution of asymmetric electrolytes [19, 20]. The MSA is a generalization of the DH approximation to finite sphere sizes and to finite particle volume fractions, and conforms to the exact Stillinger–Lovett zeroth and second order moment conditions, respectively, of local electroneutrality and charge oscillations [21, 22].

The paper is organized as follows. In section 2, we give the essentials of the simplified mode–mode coupling scheme for macroion tracer diffusion in multi-component and finite-sized electrolytes. For simplicity, we model the electrolyte solution by the restricted PM of equal sized ions with equal free diffusion coefficient D^0. In section 3, an explicit expression for the friction coefficient $\Delta\zeta_T$ and the long-time tracer diffusion coefficient D_T^L is constructed by taking advantage of simplifying properties of the linear MSA solution. The resulting expression for $\Delta\zeta_T$ is shown to be the sum of an electrostatic contribution and a charge-independent term. The appendix contains the details of the MSA static correlation functions needed for calculating $\Delta\zeta_T$. Numerical results for $\Delta\zeta_T$ and for D_T^L as functions of ionic strength, macroion–microion size ratio, macroion charge and ionic free particle mobilities are presented and discussed in section 4. This section also includes a comparison with experimental results and our concluding remarks.

2. Simplified MCS of macroion tracer diffusion

We consider an $(m+1)$-component extended primitive model consisting of an infinitely dilute tracer component, $\alpha = 0 = T$, of macroions immersed in an electrolyte solution of microionic components $\alpha = 1, \ldots, m$, solvent shear viscosity η_0 and solvent dielectric constant ϵ. A tracer macroion is characterized by its radius a_T, charge number Z_T, and its free diffusion coefficient $D_T^0 = k_B T/\zeta_T^0$ with $\zeta_T^0 = C\pi\eta_0 a_T$. The coefficient C is equal to 6 or 4, respectively, when stick or perfect slip fluid boundary conditions are assumed on the macroion surface. The microionic components have number densities $\{n_\alpha\}$ and charge numbers $\{Z_\alpha\}$. For simplicity, we assume that all microions are of the same radius a_s, and have the same free diffusion coefficient $D^0 = k_B T/(C\pi\eta_0 a_s)$.

Information on the tracer diffusion of a macroion is contained in the mean-square displacement,

$$W_T(t) = \tfrac{1}{6}\left\langle (\boldsymbol{r}_T(t) - \boldsymbol{r}_T(0))^2 \right\rangle, \tag{2}$$

of the position vector $\boldsymbol{r}_{\mathrm{T}}$ pointing to its centre. The time evolution of $W_{\mathrm{T}}(t)$ is described by the memory equation,

$$\frac{\partial}{\partial t}W_{\mathrm{T}}(t) = D_{\mathrm{T}}^{\mathrm{S}} - \frac{1}{\zeta_{\mathrm{T}}^{\mathrm{S}}}\int_0^\infty \mathrm{d}u\, \Delta\zeta_{\mathrm{T}}(t-u)\frac{\partial}{\partial u}W_{\mathrm{T}}(u), \tag{3}$$

derived from the generalized Smoluchowski equation [6–8]. The integral including the time-dependent tracer friction function, $\Delta\zeta_{\mathrm{T}}(t)$, accounts for electro-hydrodynamic retardation effects caused by the non-instantaneous response of the microion densities and associated solvent to the tracer motion. The mean-square displacement is linear in t at short and long times, respectively, with slopes $D_{\mathrm{T}}^{\mathrm{S}}$ and $D_{\mathrm{T}}^{\mathrm{L}}$ which obey the order relations $0 < D_{\mathrm{T}}^{\mathrm{L}} < D_{\mathrm{T}}^{\mathrm{S}} \leqslant D_{\mathrm{T}}^{0}$ [23].

Inspection of equation (3) shows that the time-integrated electrolyte friction contribution,

$$\Delta\zeta_{\mathrm{T}} = \int_0^\infty \mathrm{d}t\, \Delta\zeta_{\mathrm{T}}(t), \tag{4}$$

is related to $D_{\mathrm{T}}^{\mathrm{L}}$ by equation (1). The coefficient $D_{\mathrm{T}}^{\mathrm{L}}$ can be determined for a dilute macroion dispersion from a dynamic light scattering measurement of the self-dynamic scattering function

$$\begin{aligned} G_{\mathrm{T}}(q,t) &= \langle \exp\{\mathrm{i}\boldsymbol{q}\cdot(\boldsymbol{r}_{\mathrm{T}}(t) - \boldsymbol{r}_{\mathrm{T}}(0))\}\rangle \\ &= \exp\{-q^2 W_{\mathrm{T}}(t)\}\left[1 + \mathrm{O}(q^4)\right] \end{aligned} \tag{5}$$

extrapolated to zero wavenumber q and to long times [24].

The exact microscopic expression for $\Delta\zeta_{\mathrm{T}}(t)$ depends in a complicated way on the electro-steric interparticle forces, and on the many-body hydrodynamic mobility tensors of the macroion and the microions. Application of a lowest-order mode–mode coupling scheme to the microscopic expression for $\Delta\zeta_{\mathrm{T}}(t)$, and use of the Rotne–Prager (RP) far-field approximation for the hydrodynamic mobility tensors, has led to the following positive definite expression [7],

$$\frac{\Delta\zeta_{\mathrm{T}}}{\zeta_{\mathrm{T}}^{0}} = \frac{D_{\mathrm{T}}^{0}}{6\pi^2}\int_0^\infty \mathrm{d}t \int_0^\infty \mathrm{d}k\, k^4 G_{\mathrm{T}}(k,t)\boldsymbol{v}_{\mathrm{T}}(k)\cdot\boldsymbol{S}(k,t)\cdot\boldsymbol{v}_{\mathrm{T}}(k), \tag{6}$$

which approximates the increase in the tracer friction due to the presence of the electrolyte ions. We refer to [6–8] for a detailed derivation of equation (6) on the basis of the generalized Smoluchowski equation.

In equation (6), $\Delta\zeta_{\mathrm{T}}$ is expressed in terms of the dynamic self-scattering function $G_{\mathrm{T}}(k,t)$ of the tracer macroion, the symmetric $m\times m$-matrix $\boldsymbol{S}(k,t)$ of partial dynamic structure factors, $S_{\alpha\beta}(k,t)$, which describe electrolyte density correlations in the absence of the macroion, and in terms of the m-dimensional vector vertex $\boldsymbol{v}_{\mathrm{T}}(k)$ of scalar components $v_{\mathrm{T}\alpha}(k)$. The vertex vector reads explicitly

$$\boldsymbol{v}_{\mathrm{T}}(k) = \boldsymbol{c}_{\mathrm{T}}(k) - \frac{1}{D_{\mathrm{T}}^{0}}\boldsymbol{h}_{\mathrm{T}}^{\mathrm{d}}(k)\cdot\boldsymbol{S}^{-1}(k), \tag{7}$$

where the vectors $\boldsymbol{c}_{\mathrm{T}}(k)$ and $\boldsymbol{h}_{\mathrm{T}}^{\mathrm{d}}(k)$ have components $\{n_\alpha^{1/2}c_{\mathrm{T}\alpha}(k)\}$ and $\{n_\alpha^{1/2}h_{\mathrm{T}\alpha}^{\mathrm{d}}(k)\}$, respectively. Here, $c_{\mathrm{T}\alpha}(k)$ is the three-dimensional Fourier transform of the partial direct correlation function, $c_{\mathrm{T}\alpha}(r)$, and $h_{\mathrm{T}\alpha}^{\mathrm{d}}(k)$ is the distinct partial hydrodynamic function for the tracer and a microion of component α. The matrix $\boldsymbol{S}^{-1}(k)$ is the inverse of the matrix $\boldsymbol{S}(k) = \boldsymbol{S}(k,0)$ of microion partial static structure factors in the bulk electrolyte. The latter can be expressed as [23]

$$\boldsymbol{S}(k) = \boldsymbol{I} + \boldsymbol{h}(k), \tag{8}$$

where $\boldsymbol{I}$ is the identity matrix, and $\boldsymbol{h}(k)$ is an $m\times m$ matrix of components $\{(n_\alpha n_\beta)^{1/2}h_{\alpha\beta}(k)\}$ of the Fourier-transformed microion–microion total correlation functions $h_{\alpha\beta}(k)$.

Since the macroion component is assumed to be infinitely dilute, we obtain from the multi-component Ornstein–Zernike equations the following relation between the vectors of the total and direct tracer–microion correlation functions,

$$\boldsymbol{c}_{\mathrm{T}}(k) = \boldsymbol{h}_{\mathrm{T}}(k) \cdot \boldsymbol{S}^{-1}(k), \tag{9}$$

where $\boldsymbol{h}_{\mathrm{T}}(k)$ has the components $\{n_\alpha^{1/2} h_{\mathrm{T}\alpha}(k)\}$. This relation allows us to rewrite the vertex vector in the more useful form

$$\boldsymbol{v}_{\mathrm{T}}(k) = \boldsymbol{h}_{\mathrm{T}}^{\mathrm{v}}(k) \cdot \boldsymbol{S}^{-1}(k), \tag{10}$$

where we have defined a vector of associated tracer–microion vertex functions by

$$\boldsymbol{h}_{\mathrm{T}}^{\mathrm{v}}(k) = \boldsymbol{h}_{\mathrm{T}}(k) - \frac{1}{D_{\mathrm{T}}^0} \boldsymbol{h}_{\mathrm{T}}^{\mathrm{d}}(k). \tag{11}$$

The HI between tracer and microions are accounted for in (6) through the appearance of the vector, $\boldsymbol{h}_{\mathrm{T}}^{\mathrm{d}}(k)$, of distinct tracer–microion hydrodynamic functions $h_{\mathrm{T}\alpha}^{\mathrm{d}}(k)$. In the long-distance RP approximation,

$$\begin{aligned} h_{\mathrm{T}\alpha}^{\mathrm{d}}(k) &= D_{\mathrm{T}}^0 V \left\langle \hat{\boldsymbol{k}} \cdot \boldsymbol{T}_{\mathrm{T}\alpha}^{\mathrm{RP}}(\boldsymbol{r}) \cdot \hat{\boldsymbol{k}}\, \mathrm{e}^{\mathrm{i}\boldsymbol{k}\cdot\boldsymbol{r}} \right\rangle \\ &= D_{\mathrm{T}}^0 \int \mathrm{d}\boldsymbol{r}\, g_{\mathrm{T}\alpha}(r) \hat{\boldsymbol{k}} \cdot \boldsymbol{T}_{\mathrm{T}\alpha}^{\mathrm{RP}}(\boldsymbol{r}) \cdot \hat{\boldsymbol{k}}\, \mathrm{e}^{\mathrm{i}\boldsymbol{k}\cdot\boldsymbol{r}}, \end{aligned} \tag{12}$$

where V is the system volume, $\hat{\boldsymbol{k}} = \boldsymbol{k}/k$, $g_{\mathrm{T}\alpha}(r)$ is a tracer–microion radial distribution function, and $\boldsymbol{T}_{\mathrm{T}\alpha}^{\mathrm{RP}}(\boldsymbol{r})$ is the Rotne–Prager tensor [25],

$$\boldsymbol{T}_{\mathrm{T}\alpha}^{\mathrm{RP}}(\boldsymbol{r}) = a_{\mathrm{T}} \left\{ \frac{3}{4r} \left[\boldsymbol{I} + \hat{\boldsymbol{r}}\hat{\boldsymbol{r}} \right] + \frac{a_{\mathrm{T}}^2 + a_\alpha^2}{4r^3} \left[\boldsymbol{I} - 3\hat{\boldsymbol{r}}\hat{\boldsymbol{r}} \right] \right\}, \tag{13}$$

for the HI between the tracer and a macroion of radius a_α, with $\hat{\boldsymbol{r}} = \boldsymbol{r}/r$. The RP tensor is the long-distance part of the two-sphere hydrodynamic mobility tensor valid to order $1/r^3$ in the interparticle distance r. It preserves the positive definiteness of the exact many-body mobility function, and is characterized by $\nabla \cdot \boldsymbol{T}_{\mathrm{T}\alpha}^{\mathrm{RP}}(\boldsymbol{r}) = 0$ for $\boldsymbol{r} \neq 0$. In the RP approximation, the short-time tracer-diffusion coefficient $D_{\mathrm{T}}^{\mathrm{S}}$ is approximated by the Stokesian value $D_{\mathrm{T}}^0 = k_{\mathrm{B}}T/\zeta_{\mathrm{T}}^0$, and hence $\zeta_{\mathrm{T}}^{\mathrm{S}}$ by ζ_{T}^0, a fact which was used in the left-hand side of equation (6). The approximation $D_{\mathrm{T}}^{\mathrm{S}} \approx D_{\mathrm{T}}^0$ can be used for sufficiently small electrolyte volume fractions.

We expect that the RP far-field form accounts for the most important contributions of the HI between the macroions and microions. For pointlike microions, it has been shown that use of the RP approximation conforms to the exact zero-flux hydrodynamic boundary condition for a microion touching the surface of the tracer [7]. Inclusion of near-field HI contributions and lubrication forces would complicate the MCS tremendously. Moreover, it is unclear whether the lubrication theory of continuum mechanics is applicable on a length scale comparable to the size of water molecules; that is, in a situation when a (hydrated) counterion is close to the macroion surface.

Carrying out the angular integration in equation (12) and assuming microions of equal radius a_{s}, we can write the vector of partial hydrodynamic functions as

$$\boldsymbol{h}_{\mathrm{T}}^{\mathrm{d}}(k) = D_{\mathrm{T}}^0 \left\{ \int_0^\infty \mathrm{d}r\, r \boldsymbol{g}_{\mathrm{T}}(r) K_{\mathrm{T}}(k, r) \right\}, \tag{14}$$

with $\boldsymbol{g}_{\mathrm{T}}(r) = \boldsymbol{h}_{\mathrm{T}}(r) + \boldsymbol{n}^{1/2}$. The hydrodynamic kernel function, $K_{\mathrm{T}}(k, r)$, is given by

$$K_{\mathrm{T}}(k, r) = \frac{3V_{\mathrm{T}}}{2a_{\mathrm{T}}^2} \left[3 \left(j_0(kr) - \frac{j_1(kr)}{kr} \right) + \lambda''(ka_{\mathrm{T}})^2 \frac{j_2(kr)}{(kr)^2} \right]. \tag{15}$$

Here, $\boldsymbol{n}^{1/2}$ is an m-dimensional vector of microion density components $\{n_\alpha\}^{1/2}$, V_T is the volume of the macroion, $\lambda = a_\mathrm{T}/a_\mathrm{s}$ is the ratio between the macroion and microion radii, $\lambda'' = 1 + \lambda^{-2}$, and j_n is the nth order spherical Bessel function of the first kind. For later use, we note that equation (14) can be alternatively written as

$$\boldsymbol{h}_\mathrm{T}^\mathrm{d}(k) = D_\mathrm{T}^0 \left\{ \int_{a_\mathrm{T}\lambda'}^\infty \mathrm{d}r\, r \boldsymbol{h}_\mathrm{T}(r) K_\mathrm{T}(k,r) - 3V_\mathrm{T} \left(1 + \frac{3}{\lambda} + \frac{1}{\lambda^2}\right) \frac{j_1(ka_\mathrm{T}\lambda')}{ka_\mathrm{T}\lambda'} \boldsymbol{n}^{1/2} \right\}, \tag{16}$$

with $\lambda' = 1 + \lambda^{-1}$. The tracer–microion overlap region is here excluded from the integration.

The bulk dynamics of the electrolyte ions, which is independent of the tracer dynamics (but not vice versa), can be determined in principle from solving a closed set of MCS equations for $\boldsymbol{S}(k,t)$ which includes the RP form of HI for consistency [26, 27]. This elaborate and numerically demanding procedure would allow for a completely self-consistent solution for $G_\mathrm{T}(k,t)$ and hence for $\Delta\zeta_\mathrm{T}$. However, due to the modest microion correlations in the bulk, $\boldsymbol{S}(k,t)$ is expected to be only modestly perturbed from its short-time form at later times, provided that the electrolyte volume fraction is sufficiently small.

Therefore, and for analytical tractability, we approximate, in equation (6), both $\boldsymbol{S}(k,t)$ and $G_\mathrm{T}(k,t)$ by their respective short-time forms,

$$\begin{aligned} \boldsymbol{S}(k,t) &\approx \exp\{-k^2 \boldsymbol{H}(k) \cdot \boldsymbol{S}^{-1}(k) t\} \cdot \boldsymbol{S}(k) \\ G_\mathrm{T}(k,t) &\approx \exp\{-D_\mathrm{T}^0 k^2 t\}, \end{aligned} \tag{17}$$

evaluated within the RP treatment of HI. Since $D_\mathrm{T}^0 \ll D^0$ for $\lambda \gg 1$, $\boldsymbol{S}(k,t)$ decays in this case much faster than $G_\mathrm{T}(k,t)$. For $D_\mathrm{T}^0 \approx D^0$, the tracer is practically part of the electrolyte for small Z_T.

In equation (17), $\boldsymbol{H}(k)$ is an $m \times m$ matrix of partial hydrodynamic functions associated with the short-time dynamics of the microions [23]. The matrix can be split into self and distinct parts, so that

$$\boldsymbol{H}(k) = D^0 \boldsymbol{I} + \boldsymbol{H}^\mathrm{d}(k). \tag{18}$$

Note here that in the RP approximation, the short-time self-diffusion coefficient of the microions is equal to the bare diffusion coefficient D^0. The distinct part of $\boldsymbol{H}(k)$ follows in the RP approximation as [23]

$$\begin{aligned} \boldsymbol{H}^\mathrm{d}(k) &= D^0 V \left\langle \hat{\boldsymbol{k}} \cdot \boldsymbol{T}_{\alpha\beta}^\mathrm{RP}(\boldsymbol{r}) \cdot \hat{\boldsymbol{k}}\, \mathrm{e}^{\mathrm{i}\boldsymbol{k}\cdot\boldsymbol{r}} \right\rangle \boldsymbol{n}^{1/2} \boldsymbol{n}^{1/2} \\ &= D^0 \left\{ \int_0^\infty \mathrm{d}r\, r \boldsymbol{h}(r) K_\mathrm{s}(k,r) + V_\mathrm{s} \boldsymbol{n}^{1/2} \boldsymbol{n}^{1/2} \right\} \end{aligned} \tag{19}$$

where the hydrodynamic kernel function for the microions is given by

$$K_\mathrm{s}(k,r) = \frac{3V_\mathrm{s}}{2a_\mathrm{s}^2} \left[3 \left(j_0(kr) - \frac{j_1(kr)}{kr} \right) + 2(ka_\mathrm{s})^2 \frac{j_2(kr)}{(kr)^2} \right]. \tag{20}$$

The kernel $K_\mathrm{s}(k,r)$ follows from equation (15) by setting a_T equal to a_s and λ equal to one, with V_s denoting the volume of a microion sphere. In [7], the HI between the pointlike microions were fully neglected in comparison to the strong tracer–microion HI, using as justification for their neglect that $\boldsymbol{H}(k) = D^0 \boldsymbol{1} + \mathcal{O}(a_\mathrm{s}/a_\mathrm{T})$. The consideration of microion–microion HI in the present work will allow us to quantify their contribution to $\Delta\zeta_\mathrm{T}$ when the size ratio λ is not very large.

After inserting the short-time forms (17), the time integral in equation (6) is evaluated to give

$$\frac{\Delta\zeta_\mathrm{T}}{\zeta_\mathrm{T}^0} = \frac{D_\mathrm{T}^0}{6\pi^2} \int_0^\infty \mathrm{d}k\, k^2 \boldsymbol{v}_\mathrm{T}(k) \cdot \boldsymbol{S}(k) \cdot \left[D_\mathrm{T}^0 \boldsymbol{S}(k) + D^0 \boldsymbol{I} + \boldsymbol{H}^\mathrm{d}(k) \right]^{-1} \cdot \boldsymbol{S}(k) \cdot \boldsymbol{v}_\mathrm{T}(k). \tag{21}$$

We can rewrite this expression in terms of the associated tracer–microion vertex functions vector, $\boldsymbol{h}_{\mathrm{T}}^{\mathrm{v}}(k)$, defined in equation (11), and the diffusion coefficient ratio $d^2 = D^0/(D^0 + D_{\mathrm{T}}^0)$ as

$$\frac{\Delta\zeta_{\mathrm{T}}}{\zeta_{\mathrm{T}}^0} = \frac{1-d^2}{6\pi^2}\int_0^\infty \mathrm{d}k\, k^2 \boldsymbol{h}_{\mathrm{T}}^{\mathrm{v}}(k)\cdot\left[\boldsymbol{I} + \boldsymbol{h}(k) - d^2\boldsymbol{h}^{\mathrm{v}}(k)\right]^{-1}\cdot\boldsymbol{h}_{\mathrm{T}}^{\mathrm{v}}(k). \tag{22}$$

We have here defined an $m \times m$ matrix of associated microion vertex functions,

$$\boldsymbol{h}^{\mathrm{v}}(k) = \boldsymbol{h}(k) - \frac{1}{D^0}\boldsymbol{H}^{\mathrm{d}}(k). \tag{23}$$

To calculate the electrolyte friction $\Delta\zeta_{\mathrm{T}}$ from equation (22) requires as the only input the vectors $\boldsymbol{h}_{\mathrm{T}}(k)$ and $\boldsymbol{h}_{\mathrm{T}}^{\mathrm{d}}(k)$, and the matrices $\boldsymbol{h}(k)$ and $\boldsymbol{h}^{\mathrm{d}}(k)$, all of which are related to transforms of the tracer–microion and microion–microion radial distribution functions. These transforms are determined in the following section using the semi-analytical MSA solution for a multi-component PM system.

3. Explicit expressions in the mean spherical approximation

Blum and Høye [19] have provided an analytic solution for the multi-component PM in terms of the Laplace transforms,

$$\tilde{G}_{ij}(s) = \mathcal{L}\left[r g_{ij}(r)\right] = \int_0^\infty \mathrm{d}r\, r g_{ij}(r)\exp\{-sr\}, \tag{24}$$

of the partial radial distribution functions $g_{ij}(r)$ multiplied by r.

For the more special PM system we are considering here, that is, for an infinitely dilute macroion component and a host dispersion of equally sized microions, Blum and Høye's general solution simplifies considerably. A very useful simplifying property of the MSA solution in our case is that, due to the linearity of the MSA in the (Coulombic) pair potential, the radial distribution functions can be written as the sum of a hard-sphere and electrical contribution in the form

$$\begin{aligned} g_{\mathrm{T}\alpha}(r) &= \left[1 + h_{\mathrm{T}}^{\mathrm{HS}}(r)\right] + h_{\mathrm{T}}^{\mathrm{El}}(r)Z_\alpha \\ g_{\alpha\beta}(r) &= \left[1 + h^{\mathrm{HS}}(r)\right] + h^{\mathrm{El}}(r)Z_\alpha Z_\beta, \end{aligned} \tag{25}$$

where it should be noted that $h_{\mathrm{T}}^{\mathrm{El}}(r) \propto Z_{\mathrm{T}}$. In the MSA, the coupling between the density and charge fluctuations is completely neglected. Due to the linearity of the Laplace transformation, the Laplace transforms of the vector $r\boldsymbol{g}_{\mathrm{T}}(r) = r(\boldsymbol{n}^{1/2} + \boldsymbol{h}_{\mathrm{T}}(r))$ and the matrix $r\boldsymbol{g}(r) = r(\boldsymbol{n}^{1/2}\boldsymbol{n}^{1/2} + \boldsymbol{h}(r))$ are decomposable as

$$\tilde{\boldsymbol{G}}_{\mathrm{T}}(s) = \tilde{G}_{\mathrm{T}}^{\mathrm{HS}}(s)\boldsymbol{n}^{1/2} + \tilde{G}_{\mathrm{T}}^{\mathrm{EL}}(s)\boldsymbol{u} \tag{26}$$

and

$$\tilde{\boldsymbol{G}}(s) = \tilde{G}^{\mathrm{HS}}(s)\boldsymbol{n}^{1/2}\boldsymbol{n}^{1/2} + \tilde{G}^{\mathrm{EL}}(s)\boldsymbol{u}\boldsymbol{u}, \tag{27}$$

with vectors $\boldsymbol{n}^{1/2}$ and $\boldsymbol{u}$ (with components $\{n_\alpha^{1/2}\}$ and $\{n_\alpha^{1/2}Z_\alpha\}$, respectively) characterizing the densities and ionic strengths of the microion components, respectively. Here, $\tilde{G}_{\mathrm{T}}^{\mathrm{HS}}(s)$, $\tilde{G}_{\mathrm{T}}^{\mathrm{EL}}(s)$, $\tilde{G}^{\mathrm{HS}}(s)$ and $\tilde{G}^{\mathrm{EL}}(s)$ are scalar functions whose explicit analytic expressions are given in the appendix. Although there exist analytical expressions for the electrostatic and hard-sphere parts of the partial radial distribution functions in equation (25) as so-called zonal expansions [28, 20], it is possible to obtain the input functions in the MCS equation (22) directly from the Laplace transform solution without first requiring the calculation of the radial distribution function. Recognizing that

$$f(k) = \frac{4\pi}{k}\int_0^\infty \mathrm{d}r\, f(r)\sin(kr) = -\frac{4\pi}{k}\,\mathrm{Im}\left\{\tilde{f}(s = \mathrm{i}k)\right\} \tag{28}$$

for any Fourier-integrable isotropic function $f(r)$, we obtain the static input functions directly in terms of the Laplace transform solutions given in the appendix, as

$$\begin{aligned} \boldsymbol{h}_{\mathrm{T}}(k) &= h_{\mathrm{T}}^{\mathrm{HS}}(k)\boldsymbol{n}^{1/2} + h_{\mathrm{T}}^{\mathrm{EL}}(k)\boldsymbol{u} = -\frac{4\pi}{k}\,\mathrm{Im}\{\tilde{\boldsymbol{G}}_{\mathrm{T}}(\mathrm{i}k)\} \\ \boldsymbol{h}(k) &= h^{\mathrm{HS}}(k)\boldsymbol{n}^{1/2}\boldsymbol{n}^{1/2} + h^{\mathrm{EL}}(k)\boldsymbol{u}\boldsymbol{u} = -\frac{4\pi}{k}\,\mathrm{Im}\{\tilde{\boldsymbol{G}}(\mathrm{i}k)\}. \end{aligned} \tag{29}$$

The hydrodynamic input functions can be evaluated in the MSA by proceeding in the following way. First, we split them into hard-sphere and electrical parts,

$$\begin{aligned} \boldsymbol{h}_{\mathrm{T}}^{\mathrm{d}}(k) &= D_{\mathrm{T}}^{0}\left\{h_{\mathrm{T}}^{\mathrm{dHS}}(k)\boldsymbol{n}^{1/2} + h_{\mathrm{T}}^{\mathrm{dEL}}(k)\boldsymbol{u}\right\} \\ \boldsymbol{H}^{\mathrm{d}}(k) &= D^{0}\left\{h^{\mathrm{dHS}}(k)\boldsymbol{n}^{1/2}\boldsymbol{n}^{1/2} + h_{\mathrm{T}}^{\mathrm{dEL}}(k)\boldsymbol{u}\boldsymbol{u}\right\}, \end{aligned} \tag{30}$$

with

$$\begin{aligned} h_{\mathrm{T}}^{\mathrm{dHS}}(k) &= \int_0^\infty \mathrm{d}r\, r\left[1 + h_{\mathrm{T}}^{\mathrm{HS}}(r)\right] K_{\mathrm{T}}(k,r) \\ h_{\mathrm{T}}^{\mathrm{dEL}}(k) &= \int_0^\infty \mathrm{d}r\, r h_{\mathrm{T}}^{\mathrm{EL}}(r) K_{\mathrm{T}}(k,r). \end{aligned} \tag{31}$$

The scalar functions $h^{\mathrm{dHS}}(k)$ and $h^{\mathrm{dEl}}(k)$ in the matrix $\boldsymbol{h}^{\mathrm{d}}(k)$ of partial microion–microion hydrodynamic functions follow from equation (31) with the replacements $\lambda \to 1$, $\lambda' \to 2$, $K_{\mathrm{T}}(k,r) \to K_{\mathrm{s}}(k,r)$, and $h_{\mathrm{T}}^{\mathrm{HS,EL}}(r) \to h^{\mathrm{HS,EL}}(r)$.

Secondly, we express the hydrodynamic functions in terms of Blum and Høye's analytic Laplace transforms by expanding the spherical Bessel functions appearing in the hydrodynamic kernels, equations (15) and (20), in trigonometric functions. This allows us to use the relations

$$\tilde{f}^{(n)}(s) \equiv \mathcal{L}\left[\frac{f(r)}{r^n}\right] = \int_s^\infty \mathrm{d}u\, \frac{(u-s)^{n-1}}{(n-1)!}\,\tilde{f}(u), \tag{32}$$

for $n = 0, 1, 2, \ldots$ and $s > 0$, with

$$\begin{aligned} \int_0^\infty \mathrm{d}r\, \frac{f(r)}{r^n}\sin(kr) &= -\,\mathrm{Im}\{\tilde{f}^{(n)}(s = \mathrm{i}k)\} \\ \int_0^\infty \mathrm{d}r\, \frac{f(r)}{r^n}\cos(kr) &= \mathrm{Re}\{\tilde{f}^{(n)}(s = \mathrm{i}k)\}. \end{aligned} \tag{33}$$

Equation (32) follows from repeated application of the well-known Laplace transform expression $\int_s^\infty \mathrm{d}u\, \tilde{f}(u) = \mathcal{L}[f(r)/r]$.

Denoting the Laplace transform of $r\boldsymbol{g}_{\mathrm{T}}(r)/r^n$ as $\tilde{\boldsymbol{G}}_{\mathrm{T}}^{(n)}(s)$, and the Laplace transform of $r\boldsymbol{g}(r)/r^n$ as $\tilde{\boldsymbol{G}}^{(n)}(s)$, we can write the distinct hydrodynamic functions as

$$\begin{aligned} \frac{1}{D_{\mathrm{T}}^{0}}\boldsymbol{h}_{\mathrm{T}}^{\mathrm{d}}(k) = \frac{9V_{\mathrm{T}}}{2a_{\mathrm{T}}^2}\Bigg\{&-\frac{1}{k}\,\mathrm{Im}\{\tilde{\boldsymbol{G}}_{\mathrm{T}}^{(1)}(\mathrm{i}k)\} + \frac{1}{k^2}\,\mathrm{Re}\{\tilde{\boldsymbol{G}}_{\mathrm{T}}^{(2)}(\mathrm{i}k)\} + \frac{1}{k^3}\,\mathrm{Im}\{\tilde{\boldsymbol{G}}_{\mathrm{T}}^{(3)}(\mathrm{i}k)\} \\ &- \lambda''(ka_{\mathrm{T}})^2\left(\frac{1}{k^5}\,\mathrm{Im}\{\tilde{\boldsymbol{G}}_{\mathrm{T}}^{(5)}(\mathrm{i}k)\} + \frac{1}{k^4}\,\mathrm{Re}\{\tilde{\boldsymbol{G}}_{\mathrm{T}}^{(4)}(\mathrm{i}k)\} - \frac{1}{3k^3}\,\mathrm{Im}\{\tilde{\boldsymbol{G}}_{\mathrm{T}}^{(3)}(\mathrm{i}k)\}\right)\Bigg\} \end{aligned} \tag{34}$$

for the vector of tracer–microion HI contributions, and as

$$\begin{aligned} \frac{1}{D^0}\boldsymbol{H}^{\mathrm{d}}(k) = \frac{9V_{\mathrm{s}}}{2a_{\mathrm{s}}^2}\Bigg\{&-\frac{1}{k}\,\mathrm{Im}\{\tilde{\boldsymbol{G}}^{(1)}(\mathrm{i}k)\} + \frac{1}{k^2}\,\mathrm{Re}\{\tilde{\boldsymbol{G}}^{(2)}(\mathrm{i}k)\} + \frac{1}{k^3}\,\mathrm{Im}\{\tilde{\boldsymbol{G}}^{(3)}(\mathrm{i}k)\} \\ &- 2(ka_{\mathrm{s}})^2\left(\frac{1}{k^5}\,\mathrm{Im}\{\tilde{\boldsymbol{G}}^{(5)}(\mathrm{i}k)\} + \frac{1}{k^4}\,\mathrm{Re}\{\tilde{\boldsymbol{G}}^{(4)}(\mathrm{i}k)\} - \frac{1}{3k^3}\,\mathrm{Im}\{\tilde{\boldsymbol{G}}^{(3)}(\mathrm{i}k)\}\right)\Bigg\} \end{aligned} \tag{35}$$

for the matrix of microion–microion HI contributions. According to the appendix, $\tilde{\boldsymbol{G}}_{\mathrm{T}}(u)$ and $\tilde{\boldsymbol{G}}(u)$ decay exponentially for large u, and the hard-sphere parts of these functions diverge at

$u = 0$ like u^{-2}. In spite of the pole at the origin, which originates from $g_{ij}(r \to \infty) = 1$ and the asymptotic long-distance part of the HI which decays like $1/r$, this is of no consequence for calculating the hydrodynamic functions, since the small-k divergent parts of the first three transforms in equations (34) and (35) respectively, which account for the monopole (Oseen) part of HI, mutually cancel each other, leaving distinct hydrodynamic functions which are regular at $k = 0$.

The reason why we have split up all MCS-MSA input functions into a hard-sphere part proportional to $\boldsymbol{n}^{1/2}$, and an electrical part proportional to $\boldsymbol{u}$, is that the vectors $\boldsymbol{n}^{1/2}$ and $\boldsymbol{u}$ are orthogonal,

$$\boldsymbol{n}^{1/2} \cdot \boldsymbol{u} = \sum_{\alpha=1}^{m} n_\alpha Z_\alpha = 0, \tag{36}$$

because the electrolyte is overall electroneutral. A useful consequence of this orthogonality property is the possibility to evaluate the inverse matrix $\left[\boldsymbol{I} + \boldsymbol{h}(k) - d^2\boldsymbol{h}^{\mathrm{v}}(k)\right]^{-1}$ in equation (22) using the Sherman–Morrison formula [29]. Performing this matrix inversion and all dot products using equation (36) leads us to the result that, in the MCS-MSA, the electrolyte friction is given as the sum of a hard-sphere and electrical part, that is

$$\Delta\zeta_{\mathrm{T}} = \Delta\zeta_{\mathrm{T}}^{\mathrm{EL}} + \Delta\zeta_{\mathrm{T}}^{\mathrm{HS}}, \tag{37}$$

where

$$\frac{\Delta\zeta_{\mathrm{T}}^{\mathrm{EL}}}{\zeta_{\mathrm{T}}^{0}} = \frac{1-d^2}{6\pi^2}\int_0^\infty \mathrm{d}k\, k^2 \frac{u^2 (h_{\mathrm{T}}^{\mathrm{vEL}})^2}{1 + u^2 h^{\mathrm{EL}}(k) - u^2 d^2 h^{\mathrm{vEL}}(k)} \tag{38}$$

$$\frac{\Delta\zeta_{\mathrm{T}}^{\mathrm{HS}}}{\zeta_{\mathrm{T}}^{0}} = \frac{1-d^2}{6\pi^2}\int_0^\infty \mathrm{d}k\, k^2 \frac{n (h_{\mathrm{T}}^{\mathrm{vHS}})^2}{1 + n h^{\mathrm{HS}}(k) - n d^2 h^{\mathrm{vHS}}(k)}, \tag{39}$$

with associated hard-sphere tracer and microion vertex functions given by

$$\begin{aligned} h_{\mathrm{T}}^{\mathrm{vEL}}(k) &= h_{\mathrm{T}}^{\mathrm{EL}}(k) - h_{\mathrm{T}}^{\mathrm{dEL}}(k) \\ h^{\mathrm{vEL}}(k) &= h^{\mathrm{EL}}(k) - h^{\mathrm{dEL}}(k). \end{aligned} \tag{40}$$

The associated hard-sphere vertex functions are given analogously, with superscript EL replaced by HS. Here, $n = \sum_\alpha n_\alpha$ is the total microion density, $u^2 = \boldsymbol{u}\cdot\boldsymbol{u} = \kappa^2/(4\pi L_{\mathrm{B}})$, $L_{\mathrm{B}} = e^2/(\epsilon k_{\mathrm{B}} T)$ denotes the Bjerrum length of the solvent, and

$$\kappa^2 = 4\pi L_{\mathrm{B}} \sum_{\alpha=1}^{m} n_\alpha Z_\alpha^2 \tag{41}$$

defines the Debye–Hückel screening parameter κ. The electrical part in equation (37) is proportional to Z_{T}^2, since $h_{\mathrm{T}}^{\mathrm{vEL}} \propto Z_{\mathrm{T}}$, while the hard-sphere part is independent of the macroion charge. The hard-sphere part approximately determines the additional friction experienced by a (large) neutral tracer sphere immersed in a host dispersion of neutral microspheres. It depends only on d, λ, and on the total volume fraction $\phi = (4\pi/3) n a_{\mathrm{s}}^3$ of microions. The electrical part depends additionally on Z_{T}, $L_{\mathrm{B}}/a_{\mathrm{s}}$ and κa_{T}.

Equation (37) is the main result of this paper. The analytic form of this MCS-MSA expression for $\Delta\zeta_{\mathrm{T}}$ makes it amenable to a simple evaluation using a symbolic manipulation tool like *Mathematica*. Before turning to a discussion of explicit results on electrolyte friction in the following section, we first analyse here a few limiting cases of equation (37).

Ignoring HI altogether amounts to setting the tracer and microion distinct hydrodynamic functions in equation (37) to zero. Neglecting the microion distinct functions leaves us with the tracer–microion HI contribution to electrolyte friction only. The MCS equation (37) has

the desirable feature that, in the limit $\{a_T, a_s \to 0\}$ of pointlike tracer and microions, with both D^0 and D_T^0 kept finite ($d < 1$), it reduces to Onsager's limiting expression,

$$\frac{\Delta\zeta_T}{\zeta_T^0} = \frac{1}{3} L_B Z_T^2 \kappa \, (1-d) \,, \tag{42}$$

stating that the ion friction coefficient in a dilute (i.e., with κ small) and weakly charged multicomponent electrolyte increases linearly in κ [30]. Using equation (1), Onsager's limiting law reads

$$\frac{D_T^L}{D_T^0} = 1 - \frac{1}{3} L_B Z_T^2 \kappa \, (1-d) \,, \tag{43}$$

in terms of the (tracer) self-diffusion coefficient. For pure, monovalent aqueous electrolytes the limiting law is valid only up to a concentration of about 0.01 M [31].

The electrolyte friction vanishes in the limit $d \to 1$ of infinitely mobile microions, since the electrolyte atmosphere around the tracer remains spherically symmetric with respect to the tracer at each instant of time. In the limit $a_s \to 0$ of pointlike microions of finite D^0, the MSA solution in the appendix reduces to the Debye–Hückel (DH) solution for the pair distribution functions. Moreover, for pointlike microions, there is no contribution to electrolyte friction arising from microion–microion HI, since (see equation (31))

$$h^{dEL}(k) = \int_0^\infty \mathrm{d}r \, r h^{EL}(r) K_s(k,r) = 0, \tag{44}$$

and $K_s(k,r) \propto a_s$ for small a_s. Note that this conclusion remains valid even when a point-particle approximation for $h^{EL}(r)$ different from the DH approximation is used [22].

The static and hydrodynamic input functions for pointlike microions in the DH approximation are summarized in the appendix. Therein, it is further shown that $h_T^{vHS}(k) = 0$, that is

$$\left(\frac{\Delta\zeta_T}{\zeta_T^0}\right)^{HS} (a_s \to 0) = 0. \tag{45}$$

The absence of a charge-independent friction contribution for pointlike particles, when the tracer-point particle HI are treated on the RP level, follows also from exact low-density calculations. In [7], this finding was attributed to the advection of the pointlike microions in the Stokesian flow field created by the moving tracer. Neglecting tracer–microion HI gives rise to a non-zero charge-independent contribution, $(\Delta\zeta_T)^{HS}$, which, in turn, leads to a monotonic decline of D_T^L with increasing ionic strength, in conflict with experimental observation, where for colloids a minimum at $\kappa a_T \approx 0.5$ is observed. Therefore, it has been concluded that colloidal electrolyte friction must be due to a combined effect of electro-steric *and* hydrodynamic forces [7].

In the following section we will show, for finite-sized and hydrodynamically interacting microions, that the hard-sphere contribution to D_T^L is usually quite small unless the microion volume fraction is large. Under the latter circumstances the hard-sphere part of $\Delta\zeta_T$ can significantly influence the ionic-strength dependence of D_T^L.

4. Results and discussion

We first discuss charge-stabilized systems where the tracer–microion size ratio λ is much larger than 1. In figure 1, experimental data of Schumacher and van de Ven [4] for the long-time tracer diffusion coefficient, D_T^L, of polystyrene latex spheres of radius $a_T = 20$ nm, dispersed in an aqueous NaCl solution at 25 °C (with Bjerrum length $L_B = 7.1$ Å and $\eta_0 = 0.89 \times 10^{-3}$ Pa s),

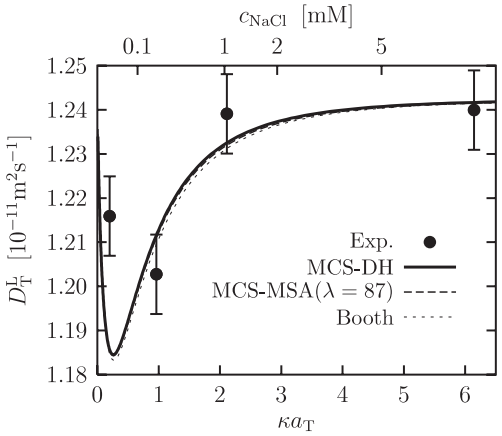

Figure 1. Long-time tracer diffusion coefficient versus κa_{T} for polystyrene spheres in an NaCl solution. Solid curve: MCS-DH for pointlike microions; long dashed curve: MCS-MSA for $\lambda = 87$; short dashed curve: Booth–Geigenmüller theory [9, 10]; symbols: dynamic light scattering data from [4].

are plotted against κa_{T}. These data are compared with the MCS-MSA prediction for finite-sized microions with $\lambda = 87$, the MSA-DH result for pointlike microions ($\lambda \to \infty$), and with Geigenmüller's correction [10] of Booth's theory of colloidal electrolyte friction [9]. In Booth's theory, finite size effects are not included, and HI are treated on an Oseen-type level of approximation. The mean radius of the microions, here consisting of Na^+ and Cl^- ions, is taken as $a_{\mathrm{s}} = (a_{\mathrm{Na^+}} + a_{\mathrm{Cl^-}})/2 = 2.3$ Å, where $a_{\mathrm{Na^+}}$ and $a_{\mathrm{Cl^-}}$ are found by applying the Stokes–Einstein relation with slip boundary conditions to the known free diffusion coefficients of these ions in water at 25 °C [32]. The free diffusion coefficient of the microions in all three schemes is then approximated to be $D^0 = 1.60 \times 10^{-9}$ m^2 s^{-1} in accord with slip boundary conditions. The free-diffusion coefficient of the tracer particles is taken to be $D_{\mathrm{T}}^0 = 1.2425 \times 10^{-11}$ m^2 s^{-1} so that $d^2 = D^0/(D^0 + D_{\mathrm{T}}^0) \approx 0.99$.

The theoretical results shown in the figure have been obtained by assuming a macroion charge number equal to $Z_{\mathrm{T}} = 165$. According to theory and experiment, the minimum (maximum) in the tracer-diffusion coefficient (electrolyte friction) appears near $\kappa a_{\mathrm{T}} \approx 0.3$ where the extension of the electric double layer, as quantified by κ^{-1}, is comparable to the diameter of the tracer. It can be seen that the inclusion of electro-steric and hydrodynamic effects due to finite-sized microions produces only a slight change in the prediction of the MCS which is most visible around $\kappa a_{\mathrm{T}} \approx 1.5$. The contribution of the MCS hard-sphere part to the electrolyte friction is negligibly small. This is consistent with the result stated earlier that $\Delta\zeta_{\mathrm{T}}^{\mathrm{HS}}$ vanishes for $a_{\mathrm{s}} \to 0$, i.e., for $\lambda \gg 1$. For the present system it should be noted that the microion volume fraction is very small even for the largest value $\kappa a_{\mathrm{T}} \approx 6$ considered in the figure (i.e., $\phi = 5 \times 10^{-4}$ for $\lambda = 87$ according to equation (A.5)).

For large λ, the microions may be treated as part of the solvent as far as the short-range part of their HI and the short-range part of their direct (i.e., excluded volume) interactions are concerned. In fact, the long-time self-diffusion coefficient of a neutral tracer sphere in a semi-dilute dispersion of host spheres is well represented by [33–35]

$$D_{\mathrm{T}}^{\mathrm{L}} = D_{\mathrm{T}}^0 \left(1 - \frac{2.5\phi}{1 + 0.16\lambda^{-1}}\right) + \mathcal{O}(\phi^2), \tag{46}$$

which demonstrates that, for large λ, $D_{\mathrm{T}}^{\mathrm{L}} \approx k_{\mathrm{B}}T/(6\pi\eta a_{\mathrm{T}})$ with $\eta = \eta_0(1 + 2.5\phi)$. As 'seen' on the length scale of the large neutral tracer, the neutral host solution acts as an effective fluid,

characterized at low host density by a viscosity η given by the Einstein result. The continuum limit for the host dispersion is practically reached when λ is larger than 10.

The MCS-DH expression for the electrolyte friction of pointlike microions is of a particularly simple and ready-to-use form. It is obtained by inserting the DH static correlation functions listed in the appendix into the electrostatic part given by equation (39). After some algebra this leads to (see equation (53) in [7])

$$\frac{\Delta\zeta_{\mathrm{T}}^{\mathrm{EL}}}{\zeta_{\mathrm{T}}^{0}} = \frac{L_{\mathrm{B}} Z_{\mathrm{T}}^2 D_{\mathrm{T}}^0}{12 a_{\mathrm{T}} D^0} F(\kappa a_{\mathrm{T}}, d), \tag{47}$$

where we have introduced the reduced electrolyte friction coefficient,

$$F(\kappa a_{\mathrm{T}}, d) = \frac{8}{\pi}(\kappa a_{\mathrm{T}})^2 d^2 \int_0^\infty \mathrm{d}y\, y^2 \frac{\overline{w}_{\mathrm{T}}(y,\kappa)^2}{\left[y^2 + (\kappa a_{\mathrm{T}})^2\right]\left[y^2 + (\kappa a_{\mathrm{T}})^2 d^2\right]}, \tag{48}$$

with

$$\overline{w}_{\mathrm{T}}(y,\kappa) = \frac{3}{2}\left[y^2 + (\kappa a_{\mathrm{T}})^2\right] \frac{\mathrm{e}^{\kappa a_{\mathrm{T}}}}{1+\kappa a_{\mathrm{T}}} f(y) - \frac{1}{1+\kappa a_{\mathrm{T}}}\left[\cos(y) + \kappa a_{\mathrm{T}} j_0(y)\right],$$

$$f(y) = \int_1^\infty \mathrm{d}x\, \mathrm{e}^{-xy}\left[j_0(xy) - \frac{j_1(xy)}{xy} + \frac{j_2(xy)}{3x^2}\right],$$

and $y = k a_{\mathrm{T}}$. The function $F(\kappa a_{\mathrm{T}}, d)$ is independent of Z_{T} and, contrary to $\Delta\zeta_{\mathrm{T}}$, it does not vanish in the limit $d \to 1$ of infinitely fast microions. Without tracer–microion HI, the MCS-DH approximation simplifies to

$$F(\kappa a_{\mathrm{T}}, d) = \frac{2\kappa a_{\mathrm{T}} d}{(1+\kappa a_{\mathrm{T}})^2}\left[1 + \frac{d-1}{d+1}\mathrm{e}^{-2\kappa a_{\mathrm{T}} d}\right]. \tag{49}$$

The leading order term in the expansion of $F(\kappa a_{\mathrm{T}}, d)$ for small $\kappa a_{\mathrm{T}} \ll 1$, i.e., for a thick double layer and dilute electrolyte, is given by

$$F(\kappa a_{\mathrm{T}} \ll 1, d) \approx \frac{2d^2}{1+d}(2\kappa a_{\mathrm{T}}) + \mathcal{O}(\kappa^2), \tag{50}$$

both with and without HI. Of course, this is just Onsager's limiting law expressed in terms of the reduced friction function $F(\kappa a_{\mathrm{T}}, d)$. Assuming pointlike microions implies $d \approx 1$ and hence $F(\kappa a_{\mathrm{T}}) \approx 2\kappa a_{\mathrm{T}}$ for small κa_{T}. For $d \approx 1$, the MCS-DH expression without HI reduces further to

$$F(\kappa a_{\mathrm{T}}, d \to 1) = \frac{2\kappa a_{\mathrm{T}}}{(1+\kappa a_{\mathrm{T}})^2}. \tag{51}$$

This functional form has a maximum with value 0.5 at $\kappa a_{\mathrm{T}} = 1$, and decays slowly for large κa_{T} like κ^{-1}. The HI between the tracer and microions strongly reduce the electrolyte friction effect. As shown in figure 2, the MCS-DH with tracer–microion HI leads to a maximum in $F(\kappa a_{\mathrm{T}}, d)$ of height 0.13, at a screening parameter $\kappa a_{\mathrm{T}} \approx 0.3$ significantly smaller than 1. Moreover, the decay of $F(\kappa a_{\mathrm{T}})$ towards zero for large κ is much faster when HI are considered (e.g., $\sim 18/(\kappa a_{\mathrm{T}})^4$ according to Booth's theory). It has been shown previously (see [7]) that the MCS-DH prediction for $F(\kappa a_{\mathrm{T}}, d \approx 1)$ with HI is very similar to the corresponding result from the Booth–Geigenmüller theory of colloidal electrolyte friction [9, 10]. This fact is exemplified in figure 2, which further includes the small-κ and large-κ asymptotic forms.

To reveal finite microion size effects, $F(\kappa a_{\mathrm{T}}, d)$ is plotted versus κa_{T} in figure 3 for various λ, with a_{s} fixed to 2.3 Å. We assume here slip ($C = 4$) and stick ($C = 6$) surface boundary conditions for the microions and for the macroion, respectively, so that $d^2 = \lambda/(\lambda + 2/3)$. Recall that $F(\kappa a_{\mathrm{T}}, d)$ calculated with linear MSA input is independent of Z_{T}. It is therefore not necessary here to specify the λ-dependence of the tracer charge.

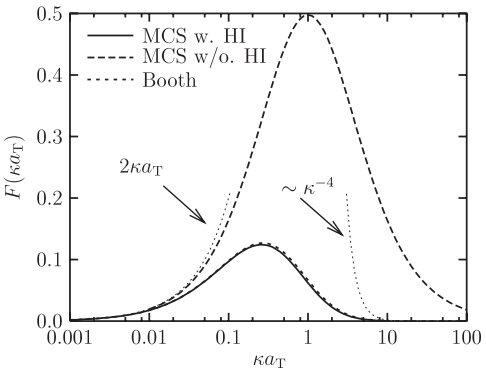

Figure 2. Reduced electrolyte friction coefficient in the MCS-DH approximation with and without HI, and in Booth–Geigenmüller theory. The parameters are the same as in figure 1. Included are the asymptotic forms for very small and very large screening parameters (dotted curves).

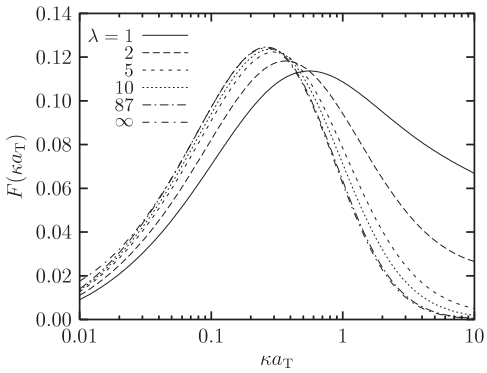

Figure 3. The MCS-MSA electrical part (i.e., the reduced colloidal friction coefficient) in aqueous electrolyte solution for various λ. The $\lambda \to \infty$ result corresponds to the DH static input.

As seen, at larger λ the only effect of the finite microion size is to shift the maximum in $F(\kappa a_T)$ to larger values of κa_T and, furthermore, to slightly reduce the friction. However, the effect is quite small even for values of λ as small as 5. Similar to related work of Vizcarra-Rendón *et al* [14], where finite size effects on colloidal electrolyte friction have been investigated on the basis of a generalized Langevin equation approach with HI ignored, the MCS-MSA scheme also shows a lessening in the large-κ decay of $F(\kappa a_T)$ both with (see figure 3) and without HI when the size ratio is decreased towards the value 1. However, in the approach of Vizcarra-Rendón *et al* the maximum in $F(\kappa a_T)$ is roughly equal to 0.5 and is located near $\kappa a_T \approx 1$, that is, the magnitude and position of the friction maximum are strongly overestimated. This observation points again to the importance of HI for the colloidal electrolyte friction effect.

In figure 4 we plot the long-time tracer diffusion coefficient for fixed microion size a_s, and varying macroion radius $a_T = \lambda a_s$. The free diffusion coefficients of the macroion and the microions are calculated from the Stokes–Einstein relation using stick and slip boundary conditions respectively, and the macroion charge is assumed to be related to the surface area, so that $Z_T = (144/86^2)(\lambda - 1)^2 + 1$. For all the size ratios plotted the hard-sphere contribution is negligible. The diffusion coefficient shows a very strong dependence on the particle charge.

Whereas the hard-sphere part in equation (37) contributes very little in the case of genuine colloidal tracer diffusion with $\lambda \gg 1$, it may significantly affect the ionic self-diffusion coefficient in the limiting case of a non-dilute symmetric mixture of monovalent microions, explored in figure 5. The hard-sphere contribution enforces here a monotonic decrease of the self-diffusion coefficient, D^L, with increasing $\kappa \propto \phi^{1/2}$. However, it should be realized for $\lambda \approx 1$ and $\phi > 0.1$ that it becomes necessary to solve the MCS self-consistently, at the expense of the simple analytic expressions given in equation (37). For the hard-sphere part in particular, it might be further necessary to invoke a hydrodynamic rescaling procedure as forwarded in [36–39], to account for many-body HI effects.

At any rate, figure 5 reconfirms, for the case of a genuine electrolyte, that the microion–microion HI contribution of the host ions to electrolyte friction is rather insignificant, even when λ is not large compared to 1. In this figure the calculated long-time tracer diffusion coefficient is shown with and without microion–microion HI (here more appropriately called

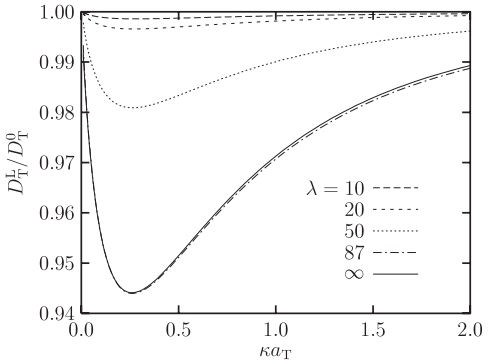

Figure 4. Long-time tracer diffusion coefficient calculated via the MCS-MSA for large λ. The macroion charge is here chosen in relation to the surface area. The $\lambda \to \infty$ result corresponds to the DH static input for $Z_T = 145$.

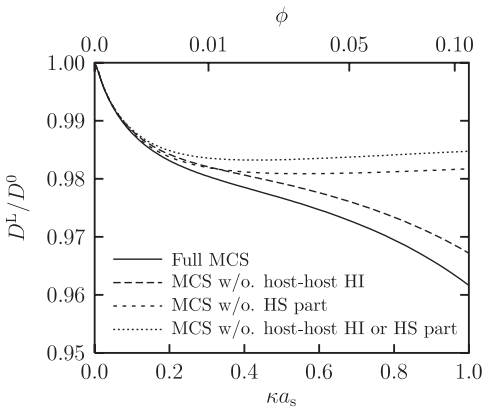

Figure 5. MCS-MSA predictions for the reduced ionic long-time self-diffusion coefficient, D^L/D^0, of a symmetric electrolyte ($\lambda = 1$ and $Z_T = 1$) of monovalent microions with $L_B/a_s = 3.09$ and $a_s = 2.3$ Å.

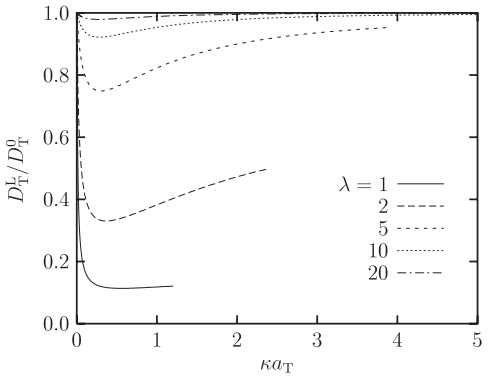

Figure 6. The normalized long-time tracer diffusion coefficient of a macroion of constant charge number $Z_T = 20$ but varying size a_T, with fixed $a_s = 2.3$ Å and $L_B/a_s = 3.09$. The curves are truncated at values of κ corresponding to a microion volume fraction of $\phi \approx 0.15$.

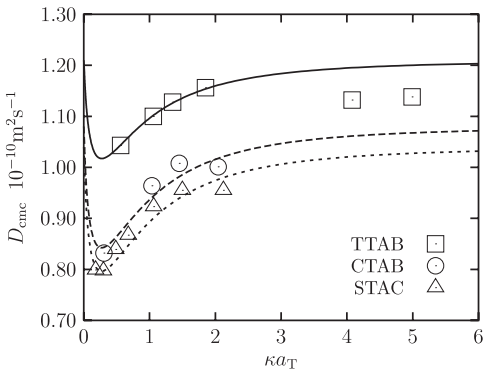

Figure 7. The long-time tracer diffusion coefficient of aqueous solutions of globular micelles at the critical micellar concentration. The squares and circles are experimental data taken from [17], the triangles are data from [18], and the curves are the MCS-MSA fits.

host–host HI, since the microions and the tracer ion are equal sized), and with and without the hard-sphere contribution included. The hard-sphere contribution becomes significant for $\phi > 0.01$ and dominates for $\phi > 0.05$. It should be pointed out, however, that the molarity of NaCl required for $\phi = 0.05$ is 1.5 M, which is far above the maximum solubility of NaCl in water.

The effect of a size-independent macroion charge on the long-time tracer diffusion coefficient is studied in figure 6. The charge on the macroion is assumed here to be fixed to $Z_T = 20$, but we again have $d^2 = \lambda/(\lambda + 2/3)$. It is seen that the electrolyte friction is strongest when the macroion size is smallest. This is due primarily to the increasing diffusivity of the strongly charged tracer ion with decreasing λ. The hard-sphere contribution is dominated by the electrical contribution.

According to Onsager's limiting law, the slope of $D_{\mathrm{T}}^{\mathrm{L}}(\kappa)$ at $\kappa = 0$ is given by

$$\frac{\mathrm{d}}{\mathrm{d}(\kappa a_{\mathrm{T}})}\left(\frac{D_{\mathrm{T}}^{\mathrm{L}}}{D_{\mathrm{T}}^{0}}\right)(\kappa = 0) = -\frac{1}{3}\left(\frac{L_{\mathrm{B}}}{a_{\mathrm{s}}}\right) Z_{\mathrm{T}}^{2}\lambda^{-1}\left(1 - \left(\frac{\lambda}{\lambda + 2/3}\right)^{1/2}\right). \qquad (52)$$

The slope becomes increasingly negative with decreasing λ. At smaller λ, the tracer macroion moves faster through its microion cloud, which causes a larger electro-hydrodynamic distortion of its surroundings and thus a stronger microion relaxation effect.

Having discussed various theoretical predictions, we finally compare the MCS-MSA scheme for tracer diffusion with experimental results for aqueous solutions of moderately charged micelles. Tominaga and Nishinaka [17, 18] have measured the long-time self-diffusion coefficient of a series of alkyltrimethylammonium-halide micelles against added salt concentration. Specifically the surfactants they have studied are tetradecyl-trimethylammonium bromide (TTAB), cetyl-trimethylammonium bromide (CTAB) and steryl-trimethylammonium chloride (STAC). The surfactant ions consist of a large head group, $(CH_3)_3N^+$, attached to an alkyl chain containing 14, 16 and 18 carbon atoms, respectively. The stretched length of the surfactant ions is 2.27, 2.53 and 2.79 nm, respectively.

The surfactants are dispersed in water with either NaCl or NaBr depending on the associated counterion of the surfactants. The self-diffusion coefficients of these ions are $1.694\times10^{-9}\,\mathrm{m^2\,s^{-1}}$ for Na^+, $2.588\times10^{-9}\,\mathrm{m^2\,s^{-1}}$ for Cl^- and $2.538\times10^{-9}\,\mathrm{m^2\,s^{-1}}$ for Br^- [32]. Assuming slip boundary conditions these coefficients correspond to the radii of 2.788, 1.818 and 1.854 Å, respectively. These radii are for the hydrated ions. The Na^+ ions effectively carry with them a hydration shell, while the larger anions do not. The anion hydrated radii are roughly equivalent to the Pauling crystalline radii. In our calculations we take the radius of the microions to be the average between the cations and anions, that is $a_{\mathrm{s}} = 2.30$ Å for NaCl and $a_{\mathrm{s}} = 2.32$ Å for NaBr. The free diffusion coefficients of the model microions are approximated using the Stokes–Einstein formula with slip boundary conditions. Figure 7 shows the MCS-MSA fit to the experimentally measured long-time diffusion coefficients of the micelles at 35 °C in water (viscosity $\eta_0 = 0.7194 \times 10^{-3}$ Pa s and Bjerrum length $L_{\mathrm{B}} = 7.25$ Å).

We assume here that the free diffusion coefficients of the micelles are also given by the Stokes–Einstein relation with slip boundary conditions. There is some evidence that one should use slip boundary conditions in the Stokes–Einstein relation when the size of the macroion is not very much larger than the one of the microions [40–42]. There are therefore only two free parameters in the fit to the experimental data, namely the tracer radius a_{T} and the micellar charge number Z_{T}. The resulting fit parameters for the three types of micelles are $a_{\mathrm{T}} = 3.89$ nm and $Z_{\mathrm{T}} = 45$ for TTAB, $a_{\mathrm{T}} = 4.36$ nm and $Z_{\mathrm{T}} = 56$ for CTAB, and $a_{\mathrm{T}} = 4.53$ nm and $Z_{\mathrm{T}} = 60$ for STAC. The difference between the fitted radii for the micelles and the stretched length of the respective surfactant ions is approximately 1.5 nm. Possible reasons for this are firstly, that not all surfactant molecules in a micelle have dissociated headgroups, secondly, there is a hydration shell formed around each micelle, and thirdly, the micelles carry associated Stern layers of essentially immobile counterions. The latter layer is not accounted for in the linearized Poisson–Boltzmann equation from which the pair correlation functions we use here are derived. The size ratio between the micelles and the model microions in all three systems is between 16 and 20. The failure of the MCS-MSA fit at high salt concentrations for the TTAB system is probably due to changes in the size and shape of a micelle due to increased surfactant aggregation. This feature is also observed in the figure for the CTAB and STAC surfactants at somewhat lower κ. Despite this behaviour the MCS-MSA describes the micellar diffusion remarkably well, particularly by accounting for the friction maximum at $\kappa a_{\mathrm{T}} \approx 0.3$. In the present micellar systems, the three size ratios are still so large that finite microion size effects are practically insignificant.

In summary, we have derived a simplified MCS with excluded volume interactions and HI between the small microions included, which compares quite well with experimental data. Using this scheme, we have found strong evidence that microionic finite size effects on macroion tracer diffusion are very small for size ratios typically larger than 10. This gives an *a posteriori* justification for the complete neglect of microion finite size influences in earlier work [7, 8]. Moreover, it allows for a simplified treatment of colloidal self-diffusion, collective diffusion [27], viscoelasticity [26] and electrophoresis of dense charge-stabilized colloidal suspensions using an extension of the present MCS scheme [43] based on earlier related work. In contrast to microion–microion HI, the influence of macroion–microion HI is crucial to the colloidal electrolyte friction effect. According to our theoretical scheme, the effect of ion–ion HI remains rather small even when considering the limiting case of self-diffusion in a genuine (symmetric) electrolyte, in accord with a corresponding finding from smart Brownian dynamics simulations [44]. However, electro-steric finite size influences are important for $\lambda \approx 1$, and need to be accounted for at larger volume fractions by a self-consistent solution of the MCS. Such a fully self-consistent calculation will be performed in future work. Finally, we would like to point out that the present MCS (and its extensions in [43]) allow us also to calculate time-dependent quantities like mean-square displacements, velocity autocorrelation functions, and frequency-dependent viscosities.

Acknowledgment

This work is supported by the Deutsche Forschungsgemeinschaft (SFB-TR6).

Appendix. MSA static pair correlation functions

The MSA solution provided by Blum and Høye [19] for the Laplace transforms of $rg_{ij}(r)$ in a general multi-component PM simplifies greatly when a restricted PM of equally sized microions with an infinitely dilute tracer component is considered. The Laplace transform of $G_{\mathrm{T}}(r) = rg_{\mathrm{T}}(r)$ is then separable in a hard-sphere and electrostatic part of the special form quoted in equation (26), with scalar functions $\tilde{G}_{\mathrm{T}}^{\mathrm{HS}}(s)$ and $\tilde{G}_{\mathrm{T}}^{\mathrm{EL}}(s)$ proportional to the hard-sphere and electrical contributions, respectively.

The hard-sphere scalar function describing tracer–microion pair correlations is given by

$$\tilde{G}_{\mathrm{T}}^{\mathrm{HS}}(s) = \frac{\mathrm{e}^{-sa_{\mathrm{T}}\lambda'}}{s^2 D_0(s)} \left[sa_{\mathrm{T}} b(\lambda) + A\right], \tag{A.1}$$

where

$$D_0(s) = 1 - 12\phi \left[A\varphi_2(2sa_{\mathrm{s}}) + B\varphi_1(2sa_{\mathrm{s}})\right]$$

$$\varphi_1(u) = \frac{(1-u) - \mathrm{e}^{-u}}{u^2}$$

$$\varphi_2(u) = \frac{\varphi_1(u)}{u} + \frac{1}{2u}$$

$$b(\lambda) = \frac{\lambda - 1}{\lambda} A + \frac{2}{\lambda} B$$

and

$$A = \frac{1 + 2\phi}{(1-\phi)^2}$$

$$B = \frac{1 + 0.5\phi}{(1-\phi)^2}.$$

Here,

$$\phi = \frac{4\pi}{3} n a_s^3, \tag{A.2}$$

is the total volume fraction of all microion components, and $n = \sum_\alpha n_\alpha$ is the total electrolyte number density. The contact distance between the tracer sphere and a microion is $a_T + a_s = a_T\lambda'$, with $\lambda' = 1 + 1/\lambda$.

The electrostatic scalar function is given by

$$\tilde{G}_T^{EL}(s) = -L_B Z_T \frac{1}{(1+2\Gamma a_T)} \frac{1}{(1+2\Gamma a_s)} \frac{e^{-s a_T \lambda'}}{s D_\pm(s)}, \tag{A.3}$$

where

$$D_\pm(s) = 1 + \frac{2\Gamma}{s} + \frac{2\Gamma^2}{s^2}\left(1 - e^{-2s a_s}\right).$$

Here, $L_B = e^2/(\epsilon k_B T)$ is the Bjerrum length and Z_T is the macroion charge number in units of elementary charges. Moreover,

$$\Gamma = \frac{1}{4a_s}\left[\sqrt{1 + 4\kappa a_s} - 1\right] \tag{A.4}$$

is the MSA screening parameter for the restricted PM of microions, which depends monotonically on the Debye–Hückel screening parameter κ. For monovalent electrolyte ions (i.e., $|Z_\alpha| = 1$ for all α),

$$(\kappa a_T)^2 = 3\left(\frac{L_B}{a_s}\right)\lambda^2 \phi, \tag{A.5}$$

which shows that $\phi \propto \lambda^{-2}$ for κa_T fixed. For $a_T = a_s$, the tracer component is part of the restricted PM of equally sized microions. Therefore, the scalar functions $\tilde{G}^{HS}(s)$ and $\tilde{G}^{EL}(s)$ in the decomposition (27) for the Laplace transform of the microion–microion pair correlations are readily obtained from equations (A.1) and (A.3) by setting a_T to a_s and λ to 1.

The MSA solution reduces to the DH solution in the limiting case of pointlike microions ($a_s = 0$), where $\phi = 0$ and $\Gamma = \kappa/2$. Then,

$$\tilde{G}_T^{HS}(s) = \frac{e^{-s a_T}}{s^2}\left[1 + s a_T\right], \tag{A.6}$$

and

$$\tilde{G}_T^{EL}(s) = -L_B Z_T \frac{e^{-s a_T}}{(1+\kappa a_T)(s+\kappa)}. \tag{A.7}$$

Using equation (28), we readily obtain for point particles,

$$h_T^{HS}(k) = -3V_T \frac{j_1(k a_T)}{k a_T}, \tag{A.8}$$

and in the DH approximation,

$$h_T^{EL}(k) = -3V_T\left(\frac{L_B}{a_T}\right)\frac{Z_T}{(k a_T)^2 + (\kappa a_T^2)}\left[\cos(k a_T) + \frac{(k a_T)(\kappa a_T)}{1+\kappa a_T} j_1(k a_T)\right]. \tag{A.9}$$

From equation (16), it follows for point particles that

$$h_T^{dHS}(k) = -3V_T \frac{j_1(k a_T)}{k a_T}, \tag{A.10}$$

since $h_T^{HS}(r) = -\Theta(a_T - r)$. Together with equations (A.8) and (40), this proves for pointlike microions that $h_T^{vHS}(k) = 0$ (see equation (45)). Finally, the electrostatic part of the total correlation function for pointlike microions follows from equation (A.9) as

$$h^{EL}(k) = -\frac{4\pi L_B}{k^2 + \kappa^2}. \tag{A.11}$$

References

[1] Verwey E J W and Overbeek J T G 1948 *Theory of the Stability of Lyophobic Colloids* (Amsterdam: Elsevier)
[2] Denton A R 1999 *J. Phys.: Condens. Matter* **11** 10061
[3] Hansen J-P and McDonald I R 1986 *Theory of Simple Liquids* 2nd edn (New York: Academic)
[4] Schumacher G A and van de Ven T G M 1987 *Faraday Discuss. Chem. Soc.* **83** 75
[5] Schumacher G A and van de Ven T G M 1991 *J. Chem. Soc. Faraday Trans.* **87** 971
[6] Nägele G and Dhont J K G 1998 *J. Chem. Phys.* **108** 9566
[7] Kollmann M and Nägele G 2000 *J. Chem. Phys.* **113** 7672
[8] Kollmann M and Nägele G 2000 *Europhys. Lett.* **52** 474
[9] Booth F 1954 *J. Chem. Phys.* **22** 1956
[10] Geigenmüller U 1984 *Chem. Phys. Lett.* **110** 666
[11] Schurr J M 1980 *Chem. Phys.* **45** 119
[12] Ruiz-Estrada H, Vizcarra-Rendón A, Medina-Noyola M and Klein R 1986 *Phys. Rev.* A **34** 3446
[13] Medina-Noyola M and Vizcarra-Rendón A 1985 *Phys. Rev.* A **32** 3596
[14] Vizcarra-Rendón A, Ruiz-Estrada H, Medina-Noyola M and Klein R 1987 *J. Chem. Phys.* **86** 2976
[15] Cruz de León G, Medina-Noyola M, Alarcón-Waess O and Ruiz-Estrada H 1993 *Chem. Phys. Lett.* **207** 294
[16] Méndez-Alcaraz J M and Alarcón-Waess O 1999 *Physica* A **268** 75
[17] Tominaga T and Nishinaka M 1993 *J. Chem. Soc. Faraday Trans.* **89** 3459
[18] Tominaga T and Nishinaka M 1995 *J. Mol. Liq.* **65/66** 333
[19] Blum L and Høye J S 1977 *J. Chem. Phys.* **81** 1311
[20] Blum L 1980 *Theoretical Chemistry: Advances and Perspectives* vol 5, ed H Eyring and D Henderson (New York: Academic) p 1
[21] Stillinger F H and Lovett R 1968 *J. Chem. Phys.* **48** 3858
[22] Attard P 1993 *Phys. Rev.* E **48** 3604
[23] Nägele G 1996 *Phys. Rep.* **272** 215
[24] Dhont J K G 1996 *An Introduction to Dynamics of Colloids* (Amsterdam: Elsevier)
[25] Rotne J and Prager S 1969 *J. Chem. Phys.* **50** 4831
[26] Nägele G and Bergenholtz J 1998 *J. Chem. Phys.* **108** 9893
[27] Nägele G, Bergenholtz J and Dhont J K G 1999 *J. Chem. Phys.* **110** 7037
[28] Henderson D and Smith W R 1978 *J. Stat. Phys.* **19** 191
[29] Press W H, Teukolsky S A, Vetterling W T and Flannery B P 1992 *Numerical Recipes* 2nd edn (Cambridge: Cambridge University Press)
[30] Onsager L 1945 *Ann. New York Acad. Sci.* **46** 241
[31] Mou C Y, Thacher T S and Lin J 1983 *J. Chem. Phys.* **79** 957
[32] Mills R and Lobo V M M 1989 *Self-Diffusion in Electrolyte Solutions* (*Physical Sciences Data* vol 36) (Amsterdam: Elsevier)
[33] Batchelor G K 1983 *J. Fluid Mech.* **131** 155
[34] Batchelor G K 1983 *J. Fluid Mech.* **137** 467 (corrigendum)
[35] Zhang H and Nägele G 2002 *J. Chem. Phys.* **117** 5908
[36] Medina-Noyola M 1988 *Phys. Rev. Lett.* **60** 2705
[37] Brady J F 1993 *J. Chem. Phys.* **99** 567
[38] Brady J F 1994 *J. Fluid Mech.* **272** 109
[39] Banchio A J, Nägele G and Bergenholtz J 1999 *J. Chem. Phys.* **111** 8721
[40] Bhattacharyya S and Bagchi B *J. Chem. Phys.* **106** 1757
[41] Ould-Kaddour F and Levesque D 2001 *Phys. Rev.* E **63** 011205
[42] Schmidt J R and Skinner J L 2003 *J. Chem. Phys.* **119** 8062
[43] McPhie M G and Nägele G 2004 work in progress
[44] Jardat M, Bernard O, Turq P and Kneller G R 1999 *J. Chem. Phys.* **110** 7993